REPORT DOCUMENTATION PAGE

Form Approved
OMB No. 0704-0188

1. REPORT DATE *(DD-MM-YYYY)*	**2. REPORT TYPE**	**3. DATES COVERED** *(From - To)*
09-06-2008	Technical Paper	

4. TITLE AND SUBTITLE

A Zero Dimensional Time-Dependent Model of High-Pressure Ablative Capillary Discharge (Preprint)

5a. CONTRACT NUMBER

5b. GRANT NUMBER

5c. PROGRAM ELEMENT NUMBER

6. AUTHOR(S)
Leonid Pekker (ERC)

5d. PROJECT NUMBER

5e. TASK NUMBER
50260542

5f. WORK UNIT NUMBER

7. PERFORMING ORGANIZATION NAME(S) AND ADDRESS(ES)

Air Force Research Laboratory (AFMC)
AFRL/RZSA
10 E. Saturn Blvd.
Edwards AFB CA 93524-7680

8. PERFORMING ORGANIZATION REPORT NUMBER

AFRL-RZ-ED-TP-2008-213

9. SPONSORING / MONITORING AGENCY NAME(S) AND ADDRESS(ES)

Air Force Research Laboratory (AFMC)
AFRL/RZS
5 Pollux Drive
Edwards AFB CA 93524-7048

10. SPONSOR/MONITOR'S ACRONYM(S)

11. SPONSOR/MONITOR'S NUMBER(S)
AFRL-RZ-ED-TP-2008-213

12. DISTRIBUTION / AVAILABILITY STATEMENT

Approved for public release; distribution unlimited (PA #08223A).

13. SUPPLEMENTARY NOTES

Submitted for presentation at the 39th AIAA Plasmadynamics and Laser Conference, to be held in Seattle, WA, 23-26 June 2008.

14. ABSTRACT

A zero-dimensional time-dependent high-pressure ($5\cdot10^6$ – $5\cdot10^8$ Pa) slab capillary discharge model is presented. The model includes a heat transfer radiation model based on a radiation database. This database has been constructed using commercially available radiation software PrismSPEC to calculate the radiation heat flux output from an uniform plasma slab. Thus, unlike earlier models, this model does not use any "asymptotic" radiation models, but self-consistently calculates the radiation heat flux at the thin transition layer, between the uniform plasma core and the ablative capillary walls. The model includes the thermodynamics of partially ionized plasmas and non-ideal effects taking place in the high-density plasma and assumes local thermodynamic equilibrium (LTE), fully dissociated plasma, no heat losses into the capillary walls, a ratio of thermal pressure to magnetic pressure much larger than unity ($\beta >> 1$), and the existence of a sonic condition at the exit plane (the plasma flow is expected to be chocked at the bore exit). The model predicts the existence of two steady-state regimes of plasma pressure for ablative discharge operation at a given plasma temperature. The first regime occurs when the plasma is so dense ($\sim 10^{26}$ m^{-3}) that the radiation mean free path, λ_{rad} is less than the slab gap of capillary, D_a, the case of super-high pressure capillary discharge.

15. SUBJECT TERMS

16. SECURITY CLASSIFICATION OF:			**17. LIMITATION OF ABSTRACT**	**18. NUMBER OF PAGES**	**19a. NAME OF RESPONSIBLE PERSON**
					Dr. Andrew Ketsdever
a. REPORT	**b. ABSTRACT**	**c. THIS PAGE**	SAR	19	**19b. TELEPHONE NUMBER** *(include area code)*
Unclassified	**Unclassified**	**Unclassified**			N/A

A Zero Dimensional Time-Dependent Model of High-Pressure Ablative Capillary Discharge (Preprint)

L. Pekker [1]
ERC Inc., Edwards AFB, CA 93524, USA

A zero-dimensional time-dependent high-pressure ($5\cdot10^6$ – $5\cdot10^8$ Pa) slab capillary discharge model is presented. The model includes a heat transfer radiation model based on a radiation database. This database has been constructed using commercially available radiation software PrismSPEC to calculate the radiation heat flux output from an uniform plasma slab. Thus, unlike earlier models, this model does not use any "asymptotic" radiation models, but self-consistently calculates the radiation heat flux at the thin transition layer, between the uniform plasma core and the ablative capillary walls. The model includes the thermodynamics of partially ionized plasmas and non-ideal effects taking place in the high-density plasma and assumes local thermodynamic equilibrium (LTE), fully dissociated plasma, no heat losses into the capillary walls, a ratio of thermal pressure to magnetic pressure much larger than unity ($\beta >>1$), and the existence of a sonic condition at the exit plane (the plasma flow is expected to be chocked at the bore exit). The model predicts the existence of two steady-state regimes of plasma pressure for ablative discharge operation at a given plasma temperature. The first regime occurs when the plasma is so dense (~ 10^{26} m^{-3}) that the radiation mean free path, λ_{rad} is less than the slab gap of capillary, D_a, the case of super-high pressure capillary discharge. The second regime occurs when the plasma density is much lower (~ 10^{24} - 10^{25} m^{-3}) such that λ_{rad} is much larger than the capillary gap, i.e. the case of moderately high plasma pressure. Both regimes converge at small plasma temperature, and there is no steady-state solution for small plasma temperatures. The calculations show that with an increase in the capillary length, the density of the plasma in the second regime ($\lambda_{rad} >> D_a$) may become so small, that the conduction heat flux to the wall becomes larger than the radiation flux to the capillary wall and transfers from the radiation mode to thermal conduction mode. We show that in this mode the capillary discharge can still exist when LTE is valid and $\beta >>1$. In the $\lambda_{rad} >> D_a$ regime the radiation heating of the wall for all capillary lengths is always a few orders of magnitude larger than conduction heating of the wall. Both regimes, radiation and thermal conduction, may be attractive for thruster applications depending on specific configurations.

I. Introduction

The role of space-based systems for both commercial and government customers continues to evolve, continually providing new requirements for the development of satellite propulsion systems. One development path is towards ever increasing power levels in a compact, efficient thruster. Being very efficient, high-pressure ablative capillary discharge is a good candidate for high-power plasma thrusters. Creating a comprehensive model of capillary discharge is important to understand the physics and engineering aspects of the capillary discharge thruster.

A schematic of a slab capillary discharge thruster is shown in Fig. 1, where D_c is the slab gap and L_c is the capillary length. The discharge maintains a resistive arc through a narrow insulating capillary by the continual ablation of the capillary wall material as shown in Fig. 1 or by injected mass. The ablative capillary discharge can be described via a three-layer configuration. The outermost layer is a solid wall, usually some form of polyethylene, occasionally Teflon or some other insulating material. Material from the wall is evaporated and enters the thin transition, or "boundary" layer, where it is dissociated, ionized, and heated to plasma temperature. The innermost layer is the plasma core. The closed end of the capillary (left side of Fig. 1) is one electrode; the other electrode

[1] Research Scientist, Leonid.Pekker.ctr@edwards.af.mil

(right side of Fig. 1) is an open end, through which the plasma can flow and expand. The polarity has no appreciable effect on discharge operation. Ohmic heating is responsible for heating, ionization, ablation, and radiation. In the model, a sonic condition ($M_a = 1$, in Fig. 1) is assumed to exist at the open end of capillary.

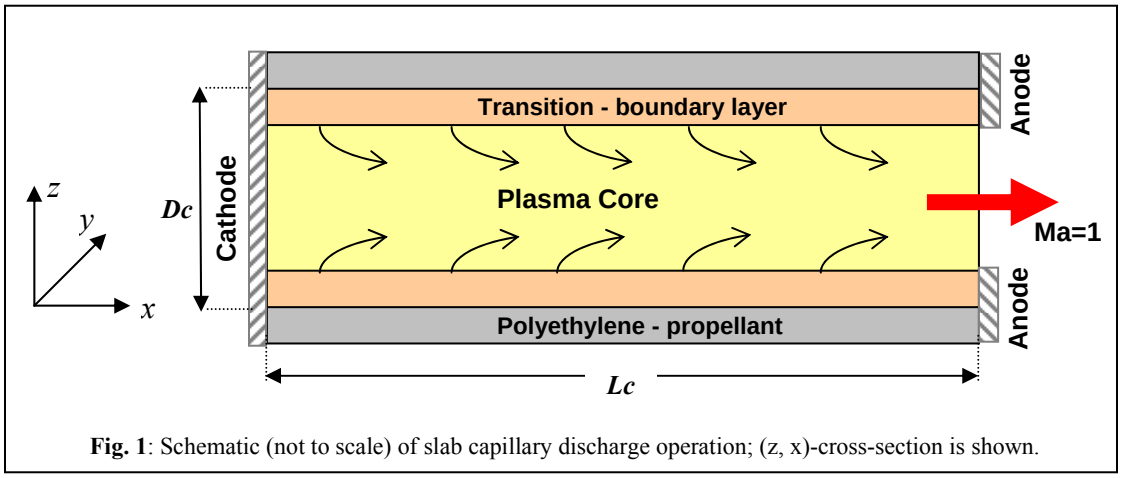

Fig. 1: Schematic (not to scale) of slab capillary discharge operation; (z, x)-cross-section is shown.

In terms of plasma propulsion concepts, the capillary plasma thruster has to satisfy two main conditions. First, the capillary plasma should be in a local thermodynamic equilibrium (LTE), indicating that all sorts of particles, electrons, ions and neutrals, have the same temperature. Then, the electrical current will heat both the elections and the heavy particles (i.e., not only the electrons), thus providing high thrust per watt. Second, as it is well known, pinching the capillary discharge leads to a formation of a narrow plasma core region with high electron temperature and a large, relatively cold peripheral plasma region. This also decreases the efficiency of the capillary thruster because only a small amount of input discharge energy is transferred to the heavy particles, with almost all of the input energy being transferred to the electrons. To minimize the pinching of the capillary discharge, the ratio of the thermal pressure to the magnetic pressure, β, in the capillary plasma thruster should be greater than unity.

The ablative capillary discharges that have been previously studied as potential electro-thermal and electro-thermo-chemical gun devices by various investigators since the mid-1980s see [1-11] and references therein, satisfy both of these conditions well. These studies investigated the dynamics of high-pressure ablative plasma discharges; they gave pressures in a range of 0.1-1 GPa and temperatures of the order of 1-3 eV. Only in recent theoretical papers[12-14] have the authors explored applications of such discharges to electro-thermal capillary thrusters.

In all theoretical models of ablative capillary discharges[1-7, 10-15] zero- and one-dimensional, the thickness of the transition layer, Fig. 1, is assumed to be negligibly small compared to the inner capillary radius and the radial distributions of plasma parameters in the plasma core, Fig. 1, are assumed to be uniform. This statement is based on the premise that the radial radiation heat transfer across the capillary chamber is so strong that it flattens the temperature and density distributions across the plasma core leading to a very thin transition layer. As it has been mentioned in [2], a strong plasma convection that might develop in the capillary discharge can also lead to flattening the capillary discharge parameters in the plasma core and thin boundary layer. Unfortunately, there exists no model of the ablative capillary discharge that would verify this premise. The main challenge for constructing such a model is a comprehensive description of the radiative heat transfer in the capillary discharge.

It is worth noting that in other types of capillary discharges operating in non-ablation regime with much faster pulses, lower pressure, high electron temperature in the plasma cores (no LTE) and $\beta < 1$, the plasma density is usually so small that thermal conduction, not radiation, is responsible for the heat transfer across the capillary and the creation non-flat radial plasma density and temperature distributions[16-19]. These discharges have been used as X-ray radiation sources in spectroscopy and lithography for wakefield acceleration and ultra-intense laser guiding. Unlike in ablative capillary discharges, in these plasma sources, capillary chambers are filled in by a gas and the capillary walls are made from a ceramic material preventing large ablation. However, as it will be shown in this work, ablative capillary discharges may also be operated in low pressure regime with thermal conduction heat larger than radiative heat (as in non-ablative capillary plasma sources), but with plasma in LTE and $\beta > 1$ as desired for propulsion applications.

The first comprehensive zero-dimensional analytical model of ablative capillary discharges was developed by Loeb and Kaplan[2]. By balancing Ohmic heating by the radiation losses, wall ablation and plasma outflow, they obtained scaling laws for the plasma temperature, pressure, wall ablation rate, and other parameters of the capillary

discharge as functions of the current, the capillary radius and length. Some key assumptions made in this model include: (1) plasma radiation is modeled as blackbody radiation; (2) the radiation flux incoming to the boundary layer (Fig. 1) ablates the wall material, dissociates, ionizes and heats ablated vapor to the plasma conditions, and no heat losses occur in the bulk wall; (3) the plasma is fully ionized; (4) when calculating the plasma enthalpy, the authors neglect the energy cost of ionization. The last assumption can be a serious error, since, for example, the carbon ions can be twice and even three times ionized and, therefore, the contribution of the ionization cost into the total plasma enthalpy can be very large, causing the dependence of enthalpy on temperature to be very different than assumed in model[2]. These simplifications allowed Loeb and Kaplan to obtain analytical solutions to the scaling laws, a significant progress at the time. However, these scaling laws are somewhat questionable, due to the level of approximations made. In further work[3-7, 10-16], the Saha equation is used to more accurately calculate the plasma composition and enthalpy of the plasma.

In the time-dependent Calligan-Mohanti zero-dimensional model[3], the rate of mass ablation $\dot{M}$ is determined by converting the radiation incident on the solid wall:

$$\dot{M} \cdot h_{vap} = F_{rad,w} \cdot A_w \quad , \tag{I.1}$$

where h_{vap} is the specific heat evaporation of the wall material; A_w is the surface area of the capillary tube; $F_{rad,w}$ is radiation heat flux incident on the insulator wall. Gilligan and Mohanti assume $F_{rad,w}$ to be a fraction f (the grey factor) of the blackbody radiation leaving the arc:

$$F_{rad,w} = f \cdot \sigma_{SB} \cdot T^4 \quad , \tag{I.2}$$

where σ_{SB} is the Stefan-Boltzmann constant and T is the temperature of plasma core, Fig. 1. Assuming local thermodynamic equilibrium and using the Saha equation, Gilligan and Mohanti calculate the internal energy of the plasma, the resistivity, and other thermodynamic parameters. To get agreement with experiments they must assume that only a small fraction ($f << 1$) of the plasma radiation reaches the wall. Thus, this model demonstrates the obvious fact that only a small fraction of the energy that has been input into the discharge is actually spent for evaporation of the wall and the main part of input energy is spent on dissociating, ionizing and heating the ablated material to plasma temperature.

In one-dimensional models[4-8, 10-11] and references therein, the authors calculate the plasma composition, resistivity, temperature, and other plasma parameters along the capillary discharge by using different levels of approximations and simplifications. However, all these models assume LTE in the plasma layer and $\beta >> 1$ and no heat losses in the bulk of the capillary walls. In [4-7, 10-11] the authors calculate the ablation mass density rate $\dot{\rho}$ averaged over the cross-section of the capillary as

$$\dot{\rho} = \frac{2 \cdot f \cdot \sigma_{SB} \cdot T^4 / R_c}{\varepsilon + P/\rho} \quad , \tag{I.3}$$

where ε, P. ρ, and T are the internal energy, plasma pressure, density and temperature in the plasma core layer; $f \cdot \sigma_{SB} \cdot T^4$ is the radiation heat flux incoming to the transition-boundary layer; and R_c is the capillary radius, while Raja-Varghese-Wilson[8] have used basically Eqs. (I.1) and (I.2).

In these models the grey factor ranges from 0.6-0.85 and 0.05-0.1 to fit experimental data depending on where authors consider the radiation flux either at the plasma-transition interface[4-7, 10-11], Eq. (I.3), or at the ablative surface[8], Eqs. (I.1) and (I.2). This indicates that plasma radiation in experiments[4, 6-8] cannot be described by a pure blackbody radiation approximation, and the Rosseland radiation mean free path λ_{rad} is larger than the capillary radius.

In works[14, 15] the authors used a different (not-blackbody-type) radiation model, a volumetric bremsstrahlang (free-free) radiation model. In their radiation models, they completely ignore the recombination (free-bound) and in-line (bound-bound) radiation processes. However, our calculation of radiation balance using PrismSPEC radiation software[20] shows that the free-bound and bound-bound electron transitions give the main contributions into the total radiation balance in high-pressure capillary. Thus, using only bremsstrahlang radiation in modeling high-pressure capillary discharge is questionable.

In a zero-dimensional ablative capillary discharge model[12] the authors have shown that steady-state ablative capillary discharge in fact may exist in two regimes. The first regime is called a super-high pressure (SHP) regime, where plasma density is assumed to be extremely high so that the plasma is opaque to its own radiation; in this case, a blackbody radiation approximation is applied. This regime corresponds to the previously developed models with the grey factor equal to one. In the second regime, the moderately high pressure (MHP) regime, the plasma density in the plasma core is assumed to be much smaller so that the plasma is completely transparent to its own radiation, but the transition layer is assumed to be opaque to the plasma radiation and to absorb all incoming radiation. In this regime, the radiation model has included bremsstrahlang (free-free) radiation and recombination (free-bound) radiation; the bound-bound radiation has been ignored. It should be stressed that the last assumption limits the applicability of this regime to the case of partially ionized plasma and multi-ionized fully ionized plasma, where the line radiation (bound-bound radiation) can be much larger than continuum radiation. However, the results obtained in this moderately high pressure regime are, probably, a valid guideline for the case of pure hydrogen (a propellant of choice for high-performance propulsion), where hydrogen plasma is assumed to be fully ionized and bound-bound radiation is absent. The prospects of ablative capillary discharges for propulsive applications are also discussed in this paper.

Thus, all previously developed models of ablative capillary discharges either consider the asymptotic radiation cases, blackbody and volumetric radiation regimes or use blackbody radiation with a grey factor to obtain agreement with the experiments; the experiments, probably, correspond to intermediate regimes, between the blackbody and volumetric regimes.

In a recent zero-dimensional high-pressure ($5\cdot10^6$ – $5\cdot10^8$ Pa) capillary discharge model[13] the authors used a radiation heat transfer model based on a radiation database. This database was constructed using commercially available radiation software PrismSPEC[20], calculating the radiation spectrum output from an uniform plasma sphere. The authors[13] applied the spectra obtained from plasma sphere with radius R_c to cylindrical capillary with the same radius since PrismSPECT does not support cylindrical symmetry. Although, such a method is not consistent (radiation from plasma sphere was used for cylindrical geometry), however, it allowed for the first time a self-consistent calculation of the radiation transport, without introducing a grey factor f, Eqs. (I.2) and (1.3). Thus, unlike previous models, model[13] did not use any "asymptotic" radiation models, but self-consistently calculates the radiation heat flux at the transition layer.

The present paper describes the high-pressure capillary discharge model[13] in detail and extends it to the case of slab geometry supported by PrismSPECT. Analysis of assumptions made in the model is given in Section II; the description of the model is presented in Section III; and numerical results and discussion are in Sections IV.

II. Model Assumptions

The following assumptions are made in the model: (1) the temperatures of electrons and heavy particles (ions and neutrals) are equal, i.e., the LTE condition is achieved; (2) plasma composition can be calculated using the Saha equation, i.e., local plasma-chemistry equilibrium is achieved; (3) heating of the plasma by the viscosity drag force is small and can be omitted from the model; (4) magnetic pressure is much smaller than thermal pressure, i.e., $\beta < 1$; (4) the the conduction heat flux is much smaller than the radiation flux and can be ignored in the model. The plasma composition and geometry assumptions are discussed in detail in Section II.F.

A. Local thermodynamic equilibrium factor (LTE-factor)

Since for typical ablative high-pressure capillary discharge, the mean free path for neutral-neutral and neutral-ion collisions are much smaller than the capillary radius (capillary slab gap D_c in slab geometry) the ions and the neutrals have the same local temperature; they are in local thermodynamic equilibrium.

In the plasma capillary core region, Fig. 1, where the plasma is usually almost fully ionized, or at least well-ionized, the electron-ion collisions play a major role in determining local thermodynamic equilibrium between electrons and heavy particles (ions and neutrals). In the electron-ion collision process the colliding particles lose or gain some energy from each other; the average exchange energy between the particles due to elastic collisions can be estimated as

$$\Delta\varepsilon_{e<=>i} \approx T\cdot\left(\frac{2\cdot m_e}{M_i}\right) \quad , \tag{II.1}$$

where T is the plasma temperature, m_e is the mass of an electron, and M_i is the ion mass. The average energy ΔW_{ei} that an electron gains from the electric field E between collisions is

$$\Delta W_{ei} = \frac{e \cdot E \cdot \mathrm{v}_{e,drift}}{\nu_{ei}} \quad , \tag{II.2}$$

where ν_{ei} is the electron-ion collision frequency, and $\mathrm{v}_{e,drift}$ is the electron drift velocity

$$\mathrm{v}_{e,drift} = \frac{e \cdot E}{m_e \cdot \nu_{ei}} \quad . \tag{II.3}$$

Substituting Eq. (II.3) into Eq. (II.2), we obtain

$$\Delta W_{ei} = \frac{e^2 \cdot E^2}{m_e \cdot \nu_{ei}^2} = 1.18 \cdot 10^{-14} \cdot \frac{E^2[V/m] \cdot T_e^3[eV]}{\Lambda_{ei}^2 \cdot Z^4 \cdot n_i^2} \quad \text{in [eV]} \; . \tag{II.4}$$

In Eq. (II.4) we have used this expression for ν_{ei}

$$\nu_{ei} = 3.94 \cdot 10^{-12} \cdot \frac{\Lambda_{ei} \cdot Z^2 \cdot n_i[m^{-3}]}{T_e^{3/2}[eV]} \quad \text{in [sec}^{-1}\text{]}, \tag{II.5}$$

taken from the NRL brochure[21]. Here, Z is the ion charge, n_i is the ion density, Λ_{ei} is the Coulomb logarithm, and $n_e = Z \cdot n_i$ is the electron number density (the plasma is assumed to be quasi-neutral). Now let us introduce the LTE-factor, K_{LTE} as the ratio of $\Delta\varepsilon_{e \Leftrightarrow i}$, Eq. (II.1), to ΔW_{ei}, Eq. (II.4):

$$K_{LTE} = \frac{\Delta\varepsilon_{e \Rightarrow i}}{\Delta W_{ei}} = 9.5 \cdot 10^{-38} \cdot \frac{n_i^2[m^{-3}] \cdot Z^4 \cdot \Lambda^2}{A_i \cdot T^2[eV] \cdot E^2[V/m]} \quad , \tag{II.6}$$

where we have substituted T for T_e in Eq. (II.4) and $M_0 \cdot A_i$ for M_i in Eq. (II.1); M_0 is the unit of atomic mass and A_i is the mass of an ion in atomic units. When this factor is large, the electron-ion collision exchange energy is larger than the average energy that the electron gains from the electric field between collisions, that is, local thermodynamic equilibrium is achieved; the electron temperature is equal to the temperature of heavy particles T. When $K_{LTE} < 1$ the electron-ion collision exchange energy is smaller than the average energy that the electron gains from the electric field between collisions, that is, there is no local thermodynamic equilibrium. In this case the electron temperature is higher than the temperature of heavy particles and is determined by balancing the energy that the electron gains from the electrical field with that transferred to ions. Thus, substituting T_e instead of T in Eq. (II.1) and setting this equation equal to Eq. (II.4) we obtain the following estimate for the electron temperature:

$$T_e[eV] \approx 3 \cdot 10^{-19} \cdot \frac{n_i[m^{-3}] \cdot Z^2 \cdot \Lambda_{ei}}{A_i^{1/2} \cdot E[V/m]} \; . \tag{II.7}$$

Obviously, the electron temperature T_e obtained this way forces K_{LTE} to equal 1. In the case of multi-ion plasma composition, Eq. (II.6) can be rewritten as

$$K_{LTE} = 9.5 \cdot 10^{-38} \cdot \frac{\Lambda_{ei}^2}{T^2[eV] \cdot E^2[V/m]} \cdot \left(\sum_k \frac{n_{i_k} \cdot Z_k^2}{A_{i_k}} \right) \cdot \left(\sum_k Z_k^2 \cdot n_{i_k} \right) \quad , \tag{II.8}$$

where index k corresponds to the ions of type k. In this equation we have averaged $1/A_i$ with the weight function equal to the collision frequency of electrons with a given type of ions,

$$\frac{1}{A_i} = \frac{\sum_k \left(\nu_{ei_k} \cdot (A_{i_k})^{-1} \right)}{\sum_k \nu_{ei_k}} \quad , \tag{II.9}$$

substituted

$$\nu_{ei} = \sum_k \nu_{ei_k} = \frac{3.94 \cdot 10^{-12}}{T_e^{3/2}[eV]} \cdot \sum_k \Lambda_{ei} \cdot Z_k{}^2 \cdot n_{i_k}[m^{-3}] \quad , \tag{II.10}$$

and, since the Coulomb logarithms for all sorts of ions are practically the same, taken Λ_{ei} out from the brackets.

Now let us consider the LTE-factor in the transition-boundary layer, Fig. 1, where the "plasma" temperature is small, about 0.3 – 1 eV, the gas is weakly ionized and, therefore, the electron-neutral collisions play the main role in the determination of the LTE in this layer. For the electron-neutral collision process the average exchange energy between neutrals and electrons is given by Eq. (II.1), where we have to substitute index *a* for index *i*:

$$\Delta\varepsilon_{e<=>a} \approx T \cdot k \cdot \left(\frac{2 \cdot m_e}{M_0} \right) \cdot \frac{1}{A_a} \quad , \qquad \frac{1}{A_a} = \frac{\sum_k \left(\frac{\nu_{ea_k}}{A_{a_k}} \right)}{\sum_k \nu_{ea_k}} = \frac{\sum_k \left(\frac{\sigma_{ea_k} \cdot n_{a_k}}{A_{a_k}} \right)}{\sum_k (\sigma_{ea_k} \cdot n_{a_k})} \quad . \tag{II.11}$$

Here n_{a_k} and σ_{ea_k} are the number density and the electron-neutral collision cross-sections for type-*k* neutral atoms. Substituting into Eqs. (II.2) and (II.3) the electron-neutral collision frequency ν_{ea_k} instead of electron-ion collision frequency ν_{ei} as

$$\nu_{ea} = \sum_k \nu_{ea_k} = V_{Te} \cdot \sum_k \left(\frac{1}{l_{ea_k}} \right) = 6.21 \cdot 10^3 \cdot \sqrt{T_e[K]} \cdot \sum_k \left(n_{a_k}[m^{-3}] \cdot \sigma_{ea_k}[m^2] \right) \quad , \tag{II.12}$$

where we have used an expression for electron thermal velocity V_{Te} ,

$$V_{Te} = \left(\frac{8 \cdot k \cdot T_e}{\pi \cdot m_e} \right) = 6.21 \cdot 10^3 \cdot \sqrt{T_e[K]} \quad , \tag{II.13}$$

we obtain the average energy ΔW_{ea} that an electron gains from the electric field *E* between collisions,

$$\Delta W_{ea} = \frac{e^2 \cdot E^2}{m_e \cdot \nu_{ea}^2} = \frac{7.3 \cdot 10^{-16} \cdot E^2}{\left(\sum_k n_{a_k} \right)^2 \cdot T} \cdot \left(\sum_k \left[\frac{n_{a_k}}{\left(\sum_k n_{a_k} \right)} \cdot \sigma_{ea_k} \right] \right)^{-2} \quad . \tag{II.14}$$

Dividing $\Delta\varepsilon_{e\Leftrightarrow a}$ by ΔW_{ea} and introducing the total pressure in the transition layer as

$$P = k \cdot T \cdot \sum_k n_{a_k}$$

(here we have neglected the small electron pressure in the transition layer), we obtain

$$K_{LTE} = 1.07 \cdot 10^{35} \cdot \frac{P^2}{E^2} \cdot \left(\sum_k \left(n_{a_k} \cdot \sigma_{ea_k} \right) \right) \cdot \frac{\sum_k \left(n_{a_k} \cdot \sigma_{ea_k} \right) \cdot \sum_k \left(\frac{\sigma_{ea_k} \cdot n_{a_k}}{A_{a_k}} \right)}{\left(\sum_k n_{a_k} \right)^2} \quad . \tag{II.15}$$

As one can see K_{LTE} in the transition layers is independent of the electron temperature; here we have assumed that the electron-neutral elastic cross-sections are independent of the electron temperature, a fair assumption for capillary discharges.

In our capillary discharge model we consider the C_4H_9 polyethylene capillary wall composition. Assuming that the gas in the transition layer is fully dissociated and using the electron-neutral collision cross-sections[4]

$$\sigma_{eC} = 2.64 \cdot 10^{-19} \ [\mathrm{m}^2] \quad \text{and} \quad \sigma_{eH} = 1.49 \cdot 10^{-19} \ [\mathrm{m}^2], \tag{II.16}$$

we obtain

$$K_{LTE, C_4H_9}^{Tran-layer} = 2.2 \cdot 10^{-3} \cdot \frac{P^2}{E^2} \quad \text{where } P \text{ in [Pa]} \quad E \text{ in [V/m]}. \tag{II.17}$$

Thus, if the LTE-factors introduced by Eqs. (II.9) and (II.17) are much larger than one, local thermodynamic equilibrium in the capillary discharge is achieved.

It should be stressed that in the case of medium ionized plasma core region, the electron-neutral collisions also must be taken into account in calculating the LTE-factor. So, Eqs. (II.1) - (II.3) can be rewritten as

$$\Delta\varepsilon_{e<=>i,a} \approx T \cdot \left(\frac{2 \cdot m_e}{M_0} \right) \cdot \frac{\sum_k \left(\nu_{ei_k} \cdot (A_{i_k})^{-1} \right) + \sum_l \left(\nu_{ea_l} \cdot (A_{a_l})^{-1} \right)}{\sum_k \nu_{ei_k} + \sum_l \nu_{ea_l}} \quad , \tag{II.18}$$

$$\Delta W = \frac{e \cdot E \cdot \mathrm{v}_{e,drift}}{\sum_k \nu_{ei_k} + \sum_l \nu_{ea_l}} \quad , \tag{II.19}$$

$$\mathrm{v}_{e,drift} = \frac{e \cdot E}{m_e \cdot (\sum_k \nu_{ei_k} + \sum_l \nu_{ea_l})} \quad . \tag{II.20}$$

where collision frequencies are given by Eqs. (II.10) and (II.12). Dividing $\Delta\varepsilon_{e\Leftrightarrow i,a}$, Eq. (II.18) by ΔW, Eq. (II.19), we obtain an expression for the LTE-factor for the case of moderately-ionized plasma core.

In our model we calculate the LTE-factor, verifying the applicability of the LTE-approximation used in the model. It should be stressed that the LTE approximation was used in all previously developed models[1-8, 10-15] but, however, without clear verification.

II.B. Local plasma-chemistry equilibrium

Let us investigate whether local ionization equilibrium in the plasma core region of high-pressure capillary discharges is achieved. Assuming an LTE in the plasma core region (the electron temperature is equal to the local temperature of heavy particles, neutrals and ions, Section II.A) the number of electron impact ionization events and the number of recombination events in three-body collisions ($i + e + e \rightarrow n + e + h\nu$) in the capillary plasma core region, Fig. 1, per unit of time can be estimated as

$$\dot{N}_{e-imp}^{ioniz} \approx n_e \cdot Exp\left(-\frac{I}{k \cdot T} \right) \cdot V_{T,e} \cdot \left(n_a \cdot \sigma_{ion} \right) \cdot V_c \quad , \tag{II.21}$$

$$\dot{N}_{3-body}^{recom} \approx \xi \cdot n_e^3 \cdot V_c \quad , \tag{II.22}$$

where I is the ionization potential; σ_{ion} is the ionization impact cross-section from the ground electronic state; $(\sigma_{ion} \cdot n_a)$ is the reverse ionization mean free path; V_c is the capillary volume; and $\xi = 8.75 \cdot 10^{-39} \cdot \mathrm{T[eV]}^{-9/2}$ is the three-body recombination coefficient[22].

The outflow of electrons through the open capillary end and together with their diffusion to the capillary wall can be estimated as

$$\dot{N}_{e,outflow} \approx n_e \cdot C_s \cdot A_c \quad , \tag{II.23}$$

$$\dot{N}_{e,diffus} \approx D_{e,diffus} \cdot \frac{n_e}{R_c} \cdot A_{wall} \approx V_{Te} \cdot \lambda_e \cdot \frac{n_e}{R_c} \cdot A_{wall} \quad , \tag{II.24}$$

where C_s,

$$C_s \approx \sqrt{\frac{\gamma \cdot P}{\rho}} = \sqrt{\frac{\gamma \cdot (n_i + n_a + n_e) \cdot k \cdot T}{(n_i + n_a) \cdot M_a}} \quad , \tag{II.25}$$

is the sound speed at the capillary open end (sonic condition, Fig. 1), A_c is the capillary cross-section area, R_c is the capillary radius (in the case of slab geometry, one-half times the slab gap D_c has to be used instead of R_c), A_{wall} is the wall area, $D_{e,diffus}$ is the electron diffusion coefficient, λ_e is the electron transport mean free path, M_a is the average mass of heavy particles, and T is the temperature of plasma core, Fig. 1. Assuming the plasma core to be fully ionized, $n_a < n_i$, $Z \approx 1$ and substituting $\gamma = 5/3$ we obtain

$$C_s \approx V_{Te} \cdot \sqrt{\frac{m_e}{M_a}} \quad . \tag{II.26}$$

When the rates of ionization and recombination events, Eq. (23) and (24), are much larger than number of electrons leaving the capillary chamber per unit of time,

$$\dot{N}_e = \dot{N}_{e,diffus} + \dot{N}_{e,outflow} \quad ,$$

we may conclude that local ionization equilibrium is achieved, i.e., the plasma composition is determined by balancing the ionization and recombination processes, resulting in Saha equilibrium. Thus, when

$$\left[1.3 \cdot 10^{-44} \cdot T[eV]^{-5} \cdot n_e^2 \ , \ Exp\left(-\frac{I}{k \cdot T} \right) \cdot \left(n_a \cdot \sigma_{ion} \right) \right] >> \\ >> \left(\frac{A_c}{V_c} \cdot \sqrt{\frac{m_e}{M_a}} + \frac{A_{wall}}{V_c} \cdot \frac{\lambda_e}{R_c} \right) \approx \left(\frac{1}{L_c} \cdot \sqrt{\frac{m_e}{M_a}} + 2.3 \cdot 10^{17} \cdot \frac{T[eV]^2}{R_c^2 \cdot \Lambda_{ee} \cdot n_e} \right) \quad , \tag{II.27}$$

the local ionization equilibrium is achieved. Here we have used Eq. (II.13) for V_{Te} and estimated λ_e [22] as

$$\lambda_e \approx 2.3 \cdot 10^{17} \cdot \frac{T[eV]^2}{\Lambda_{ee} \cdot n_e} \quad , \tag{II.28}$$

assuming that the plasma is well ionized, $n_a \sim n_i$. For typical capillary dimensions $R_c = 0.002$ m ($D_a = 4$ mm), $L_c = 0.1$ m, $n_{e,a} = 10^{25}$ m^{-3}, $T < 3$eV, $I/T \approx 5$, $\sigma_{ion} \approx 10^{-20}$ m^2 for carbon, $(m_e/M_a)^{0.5} \approx 0.007$ (for carbon) and $\Lambda_{ee} \approx 3$ we obtain, that

$$\frac{\dot{N}_{e-imp}^{ioniz}}{\dot{N}_{e,outflow} + \dot{N}_{e,diffus}} = 6.7 \cdot 10^3 \quad \text{and} \quad \frac{\dot{N}_{3-body}^{recom}}{\dot{N}_{e,outflow} + \dot{N}_{e,diffus}} = 5.4 \cdot 10^4 \quad . \tag{II.29}$$

So, for typical high-pressure ablative capillary discharge parameters, the condition of ionization equilibrium is well satisfied. Since the mean free path for heavy particles collisions is much smaller than the capillary radius for typical ablative capillary discharge, the local plasma-chemistry equilibrium is also established when the local ionization equilibrium is achieved.

Thus, it has been shown that the local plasma-chemistry equilibrium approximation is valid for high-pressure capillary discharges. This approximation is assumed in the present model as well as in all previously developed models.

It is worth noting that in the transition layer the photo-ionization processes can be more important than the electron impact ionization process due to the absorption of the large photon flux escaping from the hot plasma core region, Fig. 1, leading to an increase in the plasma temperature in this layer and larger plasma density than that calculated by the Saha formula; and second, the dissociative recombination process ($AB^+ + e \rightarrow A^* + B$) and impact-three-body recombination process with participation of a neutral as a third body ($i + e + a \rightarrow a + n + h\nu$) can also be more important than the $i + e + e \rightarrow n + e$ recombination process because the plasma in this region is weakly ionized.

II.C. Heating of the plasma by the viscosity drag force (VIS-factor)

Let us estimate the plasma heating by the viscosity drag force. We can estimate the thickness of the viscosity-boundary layer using the momentum equation for a quasi-stationary capillary discharge, Fig. 2,

$$\rho \cdot V_x \frac{\partial V_x}{\partial x} = -\frac{\partial P}{\partial x} - \eta \cdot \frac{\partial^2 V_x}{\partial z^2} \quad , \tag{II.30}$$

by setting the viscosity term equal to the left hand term of this equation:

$$\rho \cdot V_{bound} \cdot \frac{V_{bound}}{L_c} \approx \eta \cdot \frac{V_{bound}}{\delta^2} \qquad => \qquad \delta = \sqrt{\frac{L_c \cdot \eta}{\rho \cdot V_{bound}}} \quad , \tag{II.31}$$

where ρ here is the mass density of the gas in the viscosity-boundary layer, η is the viscosity coefficient, and V_{bound} is the characteristic gas velocity at the boundary of the viscosity layer, Fig. 2.

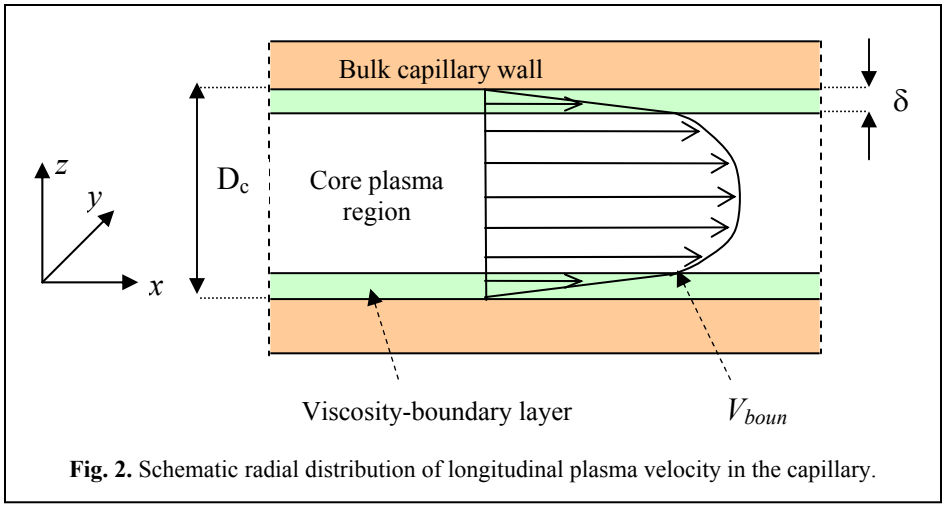

Fig. 2. Schematic radial distribution of longitudinal plasma velocity in the capillary.

The heating of the plasma due to friction forces in the viscosity-boundary layer can be estimated as

$$\dot{Q}_{visc} \approx A_{wall} \cdot \delta \cdot \eta \cdot \frac{V_{bound}}{\delta^2} \cdot V_{bound} = A_{wall} \cdot \sqrt{\frac{\eta \cdot \rho}{L_c}} \cdot V_{bound}^{5/2} \quad . \tag{II.32}$$

Substituting $\eta \approx \rho V_{Th} \cdot \lambda_{hh}$ into Eq. (II.32), where V_{Th} and λ_{hh} are the averaged thermal velocity and collision mean free path for heavy particles (neutrals and ions) in the viscosity-boundary layer, we obtain

$$\dot{Q}_{visc} = A_{wall} \cdot \rho \cdot \sqrt{\frac{V_{Th} \cdot \lambda_{hh}}{L_c}} \cdot V_{bound}^{5/2} \quad . \tag{II.33}$$

Let us estimate the rate of energy leaving the capillary through the open end, Fig. 1, as

$$\dot{Q}_{outflow} = A_c \cdot C_s \cdot h_{out} \approx A_s \cdot C_s \cdot \left(n_i \cdot u_d + c_p \cdot k \cdot T \cdot (n_a + Z \cdot n_i + n_i)\right) \quad , \tag{II.34}$$

where h_{out} is enthalpy of the plasma leaving the capillary per unit of volume, u_d is the cost per ionization, c_p, is the specific plasma heat at constant pressure. Let us introduce the viscosity factor (VIS-factor) as the ratio of the viscosity-plasma-heating-rate, Eq. (II.33) to the outgoing-energy-rate, Eq. (II.34),

$$K_{VIS} = \frac{A_{wall} \cdot \rho \cdot V_{bound}^{5/2}}{A_c \cdot C_s \cdot \left(n_i \cdot u_d + c_p \cdot k \cdot T \cdot (n_a + Z \cdot n_e + n_i)\right)} \cdot \sqrt{\frac{V_{Th} \cdot \lambda_{hh}}{L_c}} \quad . \tag{II.35}$$

If K_{VIS} factor is small, then the heating of the plasma by the viscosity drag forces is small compared to the rate of the energy leaving the capillary and can be neglected.

Substituting C_s for V_{bound}, V_{Ti} for V_{Th}, ρ as $n_i \cdot M_a$ (plasma is fully ionized), 1.66 for γ, ion-ion mean free path λ_{ii} for λ_{hh}, and one for Z, we obtain an upper estimate for VIS-factor as

$$K_{VIS} \approx \frac{A_{wall} \cdot 0.4}{A_c \cdot \left(\frac{u_d}{5 \cdot k \cdot T} + 1\right)} \cdot \sqrt{\frac{\lambda_{ii}}{L_c}} \quad . \tag{II.36}$$

Since the ion-ion mean free path is about equal to the electron-electron mean path, we can substitute Eq. (II.28) for λ_{ii} into Eq. (II.36) that gives for cylindrical capillary,

$$K_{VIS} \approx 2 \cdot 10^8 \cdot \frac{T[eV]}{R_c[m] \cdot \left(\frac{u_d[eV]}{5 \cdot T[eV]} + 1\right)} \cdot \sqrt{\frac{L_c[m]}{\Lambda_{ee} \cdot n_e[m^{-3}]}} \, . \tag{II.37}$$

Substituting typical parameters of high-pressure capillary discharge[4-7, 13]: $L_c = 0.1$ m, $R_c = 0.002$ m, $T \approx 3$ eV, $n_e \approx 10^{25}$ m^{-3}, $u_d \approx 15$ eV, $\Lambda_{ee} \approx 3$ into Eq. (II.37), we obtain that $K_{VIS} \approx 0.01$. This estimate is in good agreement with numerical results[7]. In the case of slab geometry, we have to substitute in Eq. (II.37) D_c for R_c.

Thus, it has been shown that heating of the plasma by viscosity drag forces is small and can be dropped in the modeling of high-pressure ablative capillary discharges, as it is done in the present model.

II.D. Ratio of thermal pressure to magnetic pressure (the β-factor)

The magnetic fields in both slab and cylindrical geometries can be estimated as

$$B[T] = \frac{\mu_0 \cdot J_{slab}[A/m]}{2} \qquad \text{and} \qquad B[T] = \frac{\mu_0 \cdot J_{cyl}[A]}{2 \cdot \pi \cdot R_c[m]} \quad , \tag{II.38}$$

where J_{slab} is the total capillary current per unit of slab length along the y-axis, Fig. 1, and J_{cyl} is the total current for cylindrical capillary, and μ_0 is the magnetic free-space permeability. Substituting Eqs. (III.38) into the equation for β,

$$\beta = 8 \cdot \pi \cdot 10^{-7} \cdot \frac{P[Pa]}{(B[T])^2}$$

we obtain,

$$\beta_{slab} = \frac{2 \cdot 10^7}{\pi} \cdot \frac{P[Pa]}{(J_{slab}[A/m])^2} \quad \text{and} \quad \beta_{cyl} = 2 \cdot \pi \cdot 10^7 \cdot \frac{(R_c[m])^2 \cdot P[Pa]}{(J_{cyl}[A])^2} \quad . \tag{II.39}$$

In the model, we calculate β validating a model assumption of $\beta << 1$.

II.E. Ratio of thermal conduction to radiation heat transfer (COND-factor)

One of the problems in zero-dimensional modeling of the capillary discharge is to accurately estimate the conduction heat transfer to the capillary wall or to the transition layer because the thermal conduction heat-transfer coefficient changes dramatically with the plasma-gas temperature, pressure, and plasma composition. However, in our model we estimate the radial conduction heat flux at the outer boundary of the transition layer, Fig. 1, as

$$F_{T-Cond} \approx 2 \cdot \chi_e \cdot \frac{T - T_{wall}}{D_c} \quad , \tag{II.40}$$

where

$$\chi_e = \frac{5 \cdot k^2 \cdot T \cdot n_e}{2 \cdot m_e \cdot \nu_{ee}} \qquad \text{and} \qquad \nu_{ee} = 3.6 \cdot 10^{-6} \cdot \frac{n_e[m^{-3}] \cdot \Lambda_{ee}}{(T[K])^{3/2}} \tag{II.41}$$

are the electron thermal conductivity[22] and the electron-electron collision frequency[21]; T is the temperature of the plasma core, T_{wall} is the wall temperature, n_e is the electron density in the plasma core region, Λ_{ee} is the electron Coulomb logarithm; in the case of cylindrical geometry we have to substitute $2 \cdot R_c$ for D_c. Substituting ν_{ee} into the equation for χ_e and using Eq. (II.40) we obtain that total conduction heat flows at the transition layer is

$$Q_{T-Cond} = 5.8 \cdot 10^{-10} \cdot \frac{L_c[m] \cdot (T[K])^{5/2}}{\Lambda_{ee} \cdot D_a[m]} [W/m] \quad \text{and} \quad Q_{T-Cond} = 9 \cdot 10^{-10} \cdot \frac{L_c[m] \cdot (T[K])^{5/2}}{\Lambda_{ee}} [W] \quad , \tag{II.42}$$

where the first equation corresponds to slab geometry and the second one to cylindrical capillary. In Eq. (II.42) we have dropped T_{wall}, since the plasma core temperature is usually much larger than the wall temperature or the characteristic temperature of the transition-boundary region, Fig. 1. It should be stressed that Eq. (II.42) is an upper estimate for the radial heat flux.

In the model we calculate the ratio of the radial thermal conduction heat flux, Eq. (II.42), to the radiation heat flux at the transition layer, COND-factor. When the COND-factor increases and becomes approximately one, this indicates that thermal conduction becomes comparable to the radiation heat transfer and has to be taken into account in modeling capillary discharges. Since in our model we assume no thermal conduction, our model is valid when COND-factor is much less than one.

II.F. Plasma composition and geometry assumptions

In our zero-dimensional model of ablative capillary discharge we make the following plasma composition and geometry assumptions:

1. In the model, the capillary wall is polyethylene, C_4-H_9. The radiation and plasma composition database has been constructed for this specific capillary wall composition and for 4mm slab capillary gap; we have used PrismSPECT[20] to construct our database. The chosen wall composition and slab gap are not principal; similar databases can be constructed using PrismSPECT[20] for other wall compositions and values of D_c.

2. The gas in the plasma core region is fully dissociated; this is valid for plasma temperatures large than 0.7-1 eV.

3. As in works[2-8 10-15] we neglect the heat losses into the capillary wall, assuming that all radiation heat reaching the capillary wall is spent on its ablation.

4. The temperature of the ablative gas entering into the plasma core region from the transition-boundary layer, Fig. 1, is equal to *T,* the average temperature of the capillary plasma. In other words, the plasma radiation ablates the capillary wall and then dissociates and ionizes ablated gas and finally heats it\ to the plasma temperature in the thin transition layer, Fig. 3. This assumption has been made in all previous models[1-8 10-15] and, as it has been discussed in Section I, can be verified only in a model which would include radiation heat transfer across the capillary; unfortunately, such a model does not exist yet. However, experimental observations[2, 4] do not seem to contradict this assumption.

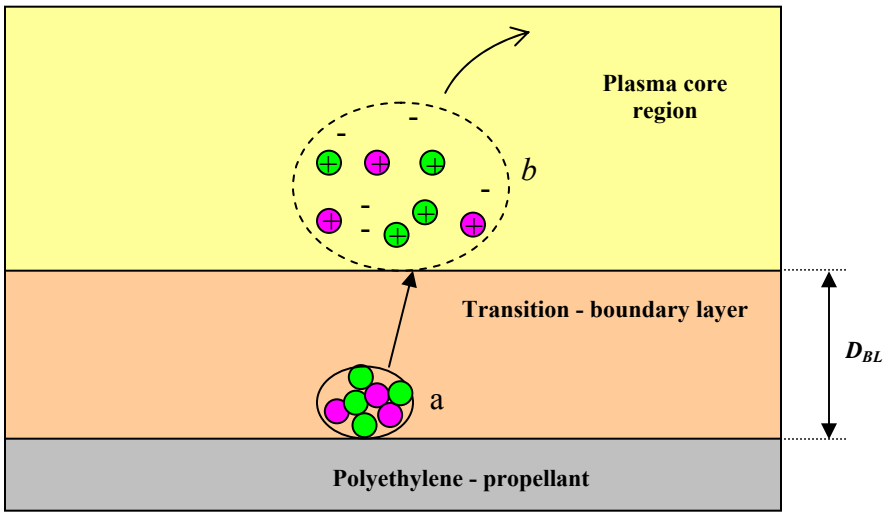

Fig. 3. Schematic of capillary discharge (not to scale) showing the transition/boundary layer between the solid wall and the plasma. Polyethylene molecules from the boiling capillary wall enter the transition layer (a) and become dissociated and ionized at the boundary between the transition layer and the plasma (b). The temperature of the particles leaving the transition layer for the plasma core region is equal to the average temperature of the plasma core; D_{BL} is the thickness of the transition layer.

III. Description of the model

III.A. Description of the database

In our model we use a radiation-plasma-composition database that has been constructed using PrismSPECT software[20]. This software calculates the plasma composition and the radiative spectral flux to the "chamber walls" for specified total number density of atoms (neutrals and ions), the element composition ratio (in our case 4 to 9 for C_4-H_9 capillary wall composition), plasma temperature, and geometry. Integrating the spectra over frequency we obtain the total radiation flux to the walls F_{rad}, which we use in our database as well as plasma composition calculated by the PrismSPECT[20]. Since PrismSPECT[20] offers only two geometries: spherical and slab (no cylindrical geometry); we have selected slab geometry, with 4mm slab gap. PrismSPECT[20] assumes an infinite slab ($L_c = \infty$); therefore, applying the calculated radiation flux to the case of limited capillary length, Fig. 1, is correct, where $L_c >> D_c$.

Preliminary PrismSPECT calculations showed that for the database selected temperatures range of 1 - 8 eV and the total number density of heavy particles between $10^{16} - 10^{28}$ m^{-3}, only H_I, H_{II}, C_I, C_{II}, C_{III}, C_{IV}, C_V, H_I (i.e. neutral atoms, ionized hydrogen and singly up to four ionized carbon atoms) contribute in plasma composition; the number densities of higher ionized carbon atom are negligibly small and are not included in the database.

It is worth noting that PrismSPECT includes free-free, free-bound, and bound-bound radiation and takes into account the pressure and Doppler broadenings of spectral lines and the reduction in ionization potential due to non-ideal plasma effects.

Applying a standard linear-interpolation method to the database we calculate the radiation flux and the plasma composition for a given plasma temperature and total number density of heavy particles (neutrals and ions).

III.B. Electrical conductivity

The electrical conductivity plays a key role in the model, by determining the rate of Joule heating. Neglecting the induced magnetic field ($\beta >> 1$), the electrical conductivity is given by:

$$\sigma = \frac{n_e e^2}{m_e(\nu_{ei}+\nu_{ea})} \quad , \tag{III.1}$$

where the electron-neutral momentum transfer collision frequency ν_{ea} given by Eqs. (II.12) with the electron collision cross-sections for neutral carbon and hydrogen atoms given by Eq. (II.16). For the electron-ion momentum transfer collision frequency ν_{ei} we used the Spitzer equation[23] modified by Zollweg-Liberman[24] in order to account for non-ideal effects,

$$\nu_{ei} = \frac{38 \cdot Z \cdot n_e \cdot e^2}{\gamma_e \cdot m_e \cdot T^{3/2}} \cdot \left(\frac{1}{2} \cdot \log\left[1 + 1.4 \cdot \Lambda_m^2\right] \right) \quad , \tag{III.2}$$

$$\Lambda_m = \frac{12 \cdot \pi \cdot \varepsilon_0 \cdot k \cdot T}{Z \cdot e^2} \cdot \left(\frac{\varepsilon_0 \cdot k \cdot T}{n_e \cdot e^2} + \left[\frac{3}{4 \cdot \pi \cdot n_i} \right]^{2/3} \right)^{1/2} \quad , \tag{III.3}$$

where $\varepsilon_0 = 8.854 \cdot 10^{-12}$ [F/m] is the permittivity of free space, and the factor $\gamma_e(Z)$ in is a weak function of average ion charge Z and can be approximated as [4] $\gamma_e \approx 0.58 + 0.1 \cdot (Z\text{-}1)$. It should be noted that Eq. (III.2) differs from Eq. (II.5) for ν_{ei}. However, in the case where the non-ideal effects are negligibly small, the plasma density is bellow than 10^{24} m^{-3}, Eq. (III.2) converges to Eq. (II.5). Since for typical high-pressure capillary discharges the no-ideal effects are rather small (differences in calculating ν_{ei} by Eqs. (II.5) and (III.3) are less than 30%) using Eq. (II.5) to calculate the LTE-factor is acceptable. However, to calculate plasma resistance we have to use the more accurate formula for ν_{ei}.

III.C. Equation for ablation rate of the capillary wall, plasma enthalpy

Calculating a required enthalpy h_{CH} to bring a "C_4H_9 polyethylene molecule" from the capillary wall to the plasma region, Fig. 3, is another key aspect of the model. Introducing the ablation rate of the capillary wall material as a number of "C_4H_9 molecules" incoming in the capillary chamber per unit of time per unit of the slab length along the y-axis, Fig. 1, we obtain

$$\dot{N}_{CH}^{in} = \frac{2 \cdot F_{rad} \cdot L_c}{h_{CH}} \quad , \tag{III.4}$$

where F_{rad} is the radiation flux at the boundary-transition layer. The enthalpy h_{CH} is

$$h_{CH} = \Delta\varepsilon_\Phi + C_p \cdot k \cdot T \cdot (1 + Z \cdot \varphi) \cdot (C_\alpha + H_\alpha) \quad , \tag{III.5}$$

where $C_\alpha = 4$, $H_\alpha = 9$, $\Delta\varepsilon_\Phi$ includes the energies of vaporization, dissociation, ionization, and electronic excitation, $C_P = \gamma/(\gamma + 1)$ is the specific heat at constant pressure with γ=5/3, and $\varphi = n_i/(n_i + n_a)$ is the ionization ratio. The vaporization and dissociation energies are considered as constants in the model and are input parameters in the code. It is worth noting again that in the model we neglect the radiation heating of bulk capillary wall, assuming that all radiation incoming into the transition layer is absorbed into this region and expended on the ablation of wall material, as stated in Eq. (III.4).

Calculating electronic excitation energy we take into account (1) 16, 12, 6, 4, 1, 4 and 1 pseudo-levels (i.e. groups of elementary levels with combined statistical degeneracy) and average energy – for C_I, C_{II}, C_{III}, C_{IV}, C_V, H_I, and H_{II} respectively; the contributions of higher numbers of electron-partition functions into plasma enthalpy is negligibly small; and (2) the reduction in the ionization potentials due to the non-ideality of the plasma. In non-ideal plasmas the ionization potential decreases because in dense plasmas "free" electrons are no longer completely free (like in an ideal plasmas) but remain weakly bound to the ions (not to the neutrals). Therefore, less energy is required to remove an electron to a weakly bond state (from which the electron can then easily escape, obtaining the necessary small amount of energy from elsewhere) than to a completely free state. The reduction in the ionization potential of l-ionized atom[4, 25-27] is

$$\Delta I_{l->l+1} = \frac{l \cdot e^2}{4 \cdot \pi \cdot \varepsilon_0 \cdot \left(\lambda_D + \frac{\Omega}{8} \right)} = \frac{l \cdot 1.44 \cdot 10^{-9}}{\left(\lambda_D + \frac{\Omega}{8} \right)} \ [eV] \quad , \tag{III.6}$$

where λ_D is the Debye length and Ω is the deBroglie wavelength:

$$\lambda_D = 6.9 \cdot 10^1 \cdot \left[\frac{T[K]}{(1+Z) \cdot n_e[m^3]} \right]^{1/2} [m] \quad , \tag{III.7}$$

$$\Omega = \frac{h}{\left(2 \cdot \pi \cdot k \cdot m_e \cdot T\right)^{1/2}} = 7.45 \cdot 10^{-8} \cdot \left(T[K]\right)^{-1/2} \ [m] \quad . \tag{III.8}$$

Here both the electron and positive-ion shielding are taken into account. For neutral atoms, l is equal to zero (they do not attract negative particles as well as positive ions) so there is no reduction in their ionization potentials. Substituting $n_e = 6 \cdot 10^{26}$ m^{-3}, $T = 4$ eV and $Z = 1$, into Eqs. (IV.1) – (IV.3), we obtain $\Delta I_{l \to l+1} \approx l \cdot 0.3$ eV. We would like to note that since the Coulomb interaction is negative, the plasma pressure is reduced too because the electrons spend some time near ions not bombarding a "chamber wall". As has been shown[12, 27], this reduction is less than 10% relative to the total plasma pressure for our conditions. Therefore, we neglect the pressure reduction in our model.

Thus, for a given plasma temperature and heavy particle number density we find the plasma composition and radiation flux at the transition layer, F_{rad}. Then, using plasma composition we calculate: the average ion charge Z; the ionization energies while accounting for the reductions in ionization potentials of heavy particles; populations of electronic levels of carbon and hydrogen ionized and neutral atoms by employing the Saha equation; and finally $\Delta\varepsilon_\Phi$ and then h_{CH}. Substituting F_{rad} and h_{CH} into Eq. (III.3) we calculate the ablation rate of wall material.

We have to stress that in Eq. (III.5) we have neglected the kinetic (not thermal) energy of the ablated materials incoming into the plasma region. This is a correct assumption since the capillary length L_c is assumed to be much larger than the slab gap D_c, Fig. 1.

III.D. Mass and energy equations

An equation describing the outflow of ablated "polyethylene molecules" through the open capillary end, Fig. 1, can be written as

$$\dot{N}_{CH}^{out} = n_{CH,end} \cdot D_{slab} \cdot C_{s,end} \quad , \tag{III.9}$$

with

$$C_{s,end} = \left(\frac{\gamma \cdot P_{end}}{\rho_{end}} \right)^{1/2} = \left(\frac{\gamma \cdot (1 + Z_{end} \cdot \varphi_{end}) \cdot k \cdot T_{end}}{\overline{M}} \right)^{1/2} \quad , \tag{III.10}$$

$$\overline{M} = \frac{C_\alpha \cdot M_C + H_\alpha \cdot M_H}{C_\alpha + H_\alpha} \quad , \tag{III.12}$$

where index "*end*" denotes conditions at the exit plane and the absence of the index "*end*" denotes conditions averaged over the capillary volume, in the "middle" of capillary. Here n_{CH} is the mole number density of ablated molecules and M_C and M_H are carbon and hydrogen atomic masses respectively.

Combing Eqs. (III.4) and (III.9) and using the isentropic flow relations[28] and assuming that average ion charge and ionization ratio are preserved through the capillary up to the exit plane, $Z_{end} = Z$ and $\varphi_{end} = \varphi$, we obtain the following equation for the law of conservation of mass:

$$D_c \cdot L_c \cdot \frac{dn_{CH}}{dt} = \frac{2 \cdot F_{rad}(n_{CH}, T) \cdot L_c}{h_{CH}(n_{CH}, T)} - \Gamma \cdot n_{CH} \cdot D_c \cdot C_s \quad , \tag{III.13}$$

where

$$\Gamma = \left(\frac{2}{\gamma + 1} \right)^{\frac{\gamma+1}{2(\gamma+1)}} \quad . \tag{III.14}$$

Since we assume that there is no energy loss in the capillary discharge, we may conclude that all electrical energy put into the capillary discharge is leaving the capillary with the plasma jet at the exit plane or is expended on increasing the inner energy of the plasma inside the capillary. This gives the following equation for the law of conservation of energy:

$$D_c \cdot L_c \cdot \frac{d(n_{CH} \cdot \varepsilon_{CH})}{dt} = \frac{(J_{slab})^2 \cdot L_c}{D_c \cdot \sigma} - \Gamma \cdot n_{CH} \cdot D_c \cdot C_s \cdot h_{CH}(n_{CH}, T) \, , \tag{III.15}$$

where ε_{CH} is the inner plasma energy,

$$h_{CH} - \varepsilon_{CH} = k \cdot T \quad . \tag{III.16}$$

Thus, solving Eqs. (III.13) and (III.15) for a given $J_{slab}(t)$ and initial plasma conditions, $n_{CH}(t = 0)$ and $T(t = 0)$, we obtain all characteristics of capillary discharge vs. time. It has to be mentioned that the authors[13] used a similar system of equation for cylindrical capillaries investigating the stability of the capillary discharge for the case of J_{slab}=const and different initial plasma conditions. They also calculated the discharge parameters employing LRC circuit to self-consistently calculate the current and compared obtained results with experiments.

IV. Numerical results and discussions

In the numerical results presented below, the database temperature and C_4H_9-mole number density were 1 – 8 Ev, and $7.7 \cdot 10^{14}$ -$7.7 \cdot 10^{16}$ m-3, the energy of evaporation and dissociation were taken as zero (for polyethylene[2] they are much smaller than ionization potentials of carbon and hydrogen, and since the ionization ratio of the plasma is larger than 15%, Fig. 4, they can be ignored) The capillary lengths were chosen as 4, 6, and 10 cm, and D_c was 4 mm. In this paper we investigate the steady-state solutions of Eqs. (III.13) and (III.15). As shown in Figs. 4 - 10, the model predicts the existence of two steady-state regimes for ablative discharge operation at a given plasma temperature. The first regime occurs with the plasma is so dense that the radiation mean free path λ_{rad} is smaller than or equal to about the capillary gap, the case of super-high pressure (SHP) capillary discharge, solid curves in Figs. 4 - 10, and the second case occurs with the plasma density much lower such that λ_{rad} is much larger than D_c, i.e. the case of moderately high pressure (MHP) capillary discharge, dashed curves. As shown in Figs. 4 – 10, the regimes converge at small plasma temperature, and there are no steady-state solutions for plasma temperatures smaller than 1.215, 1.43, and 1.74 for L_c = 4, 6, and 10 cm, respectively. In the SHP- regime the pressure range is $10^7 – 5 \cdot 10^8$ Pa, and in MHP-regime pressures are much smaller than $10^5 – 10^6$ Pa, Fig.5, and, therefore the ionization ratio is larger for SHP-regime than for MHP-regime at the same plasma temperature, Fig. 4.

Fig. 6 shows the ratio of radiation flux at the transition layer, Fig. 1, to the blackbody radiation flux with the same plasma temperature. As one can see the gray factor *f*, Eq. (I.3), varies from 0.1 to almost 1 for the SHP-regime and from 0.23 to 0.03 for the MHP-regime depending of plasma temperature and the capillary length. This indicates

that the grey factor may change noticeably with time in non-steady operation regime and, therefore, to assume it is constant (as has been done in models[2-8, 10, 11]) can leads to false results. The current, power, and capillary wall ablation rate per one meter of capillary length in the y-direction are shown in Fig. 7, 8, and 9. As one can see the parameters of capillary discharges may differ more than one order of magnitude or even as much two orders for SHP- and MHP-regime.

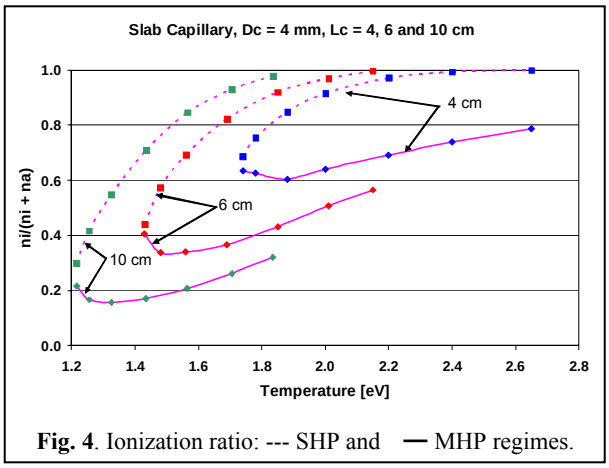

Fig. 4. Ionization ratio: --- SHP and — MHP regimes.

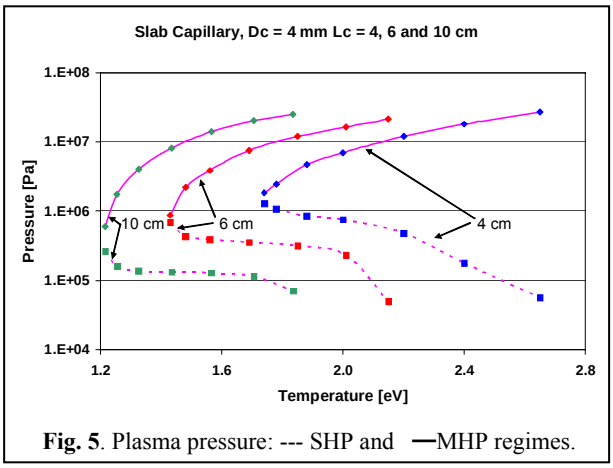

Fig. 5. Plasma pressure: --- SHP and —MHP regimes.

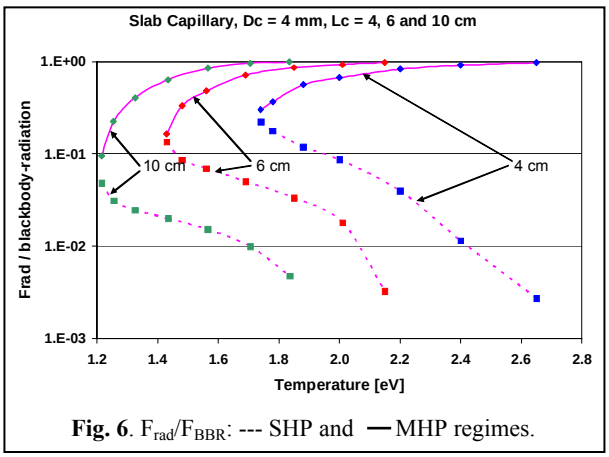

Fig. 6. F_{rad}/F_{BBR}: --- SHP and — MHP regimes.

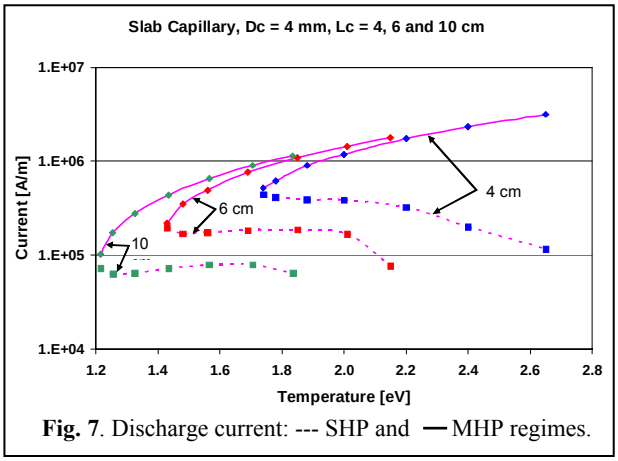

Fig. 7. Discharge current: --- SHP and — MHP regimes.

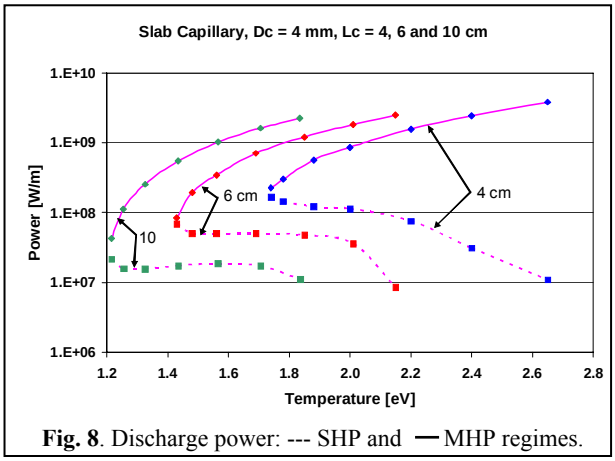

Fig. 8. Discharge power: --- SHP and — MHP regimes.

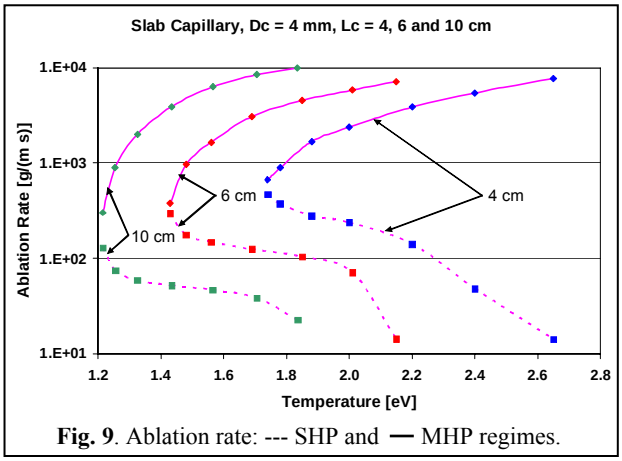

Fig. 9. Ablation rate: --- SHP and — MHP regimes.

Figs. 10 – 12 show the dependence of the LTE-factor, β, and the COND-factor vs. temperature for both regimes. As one can see the SHP-regime satisfies all three assumptions of the model: the LTE-factor and β are much larger than one, and the COND-factor is much smaller than one in all temperature regions. However, the MHP-regime satisfies

only two of the model assumptions: the LTE-factor and β are much larger than one in all temperature regions, while the COND-factor in this regime increases with temperature and becomes larger than 1, Fig. 12.

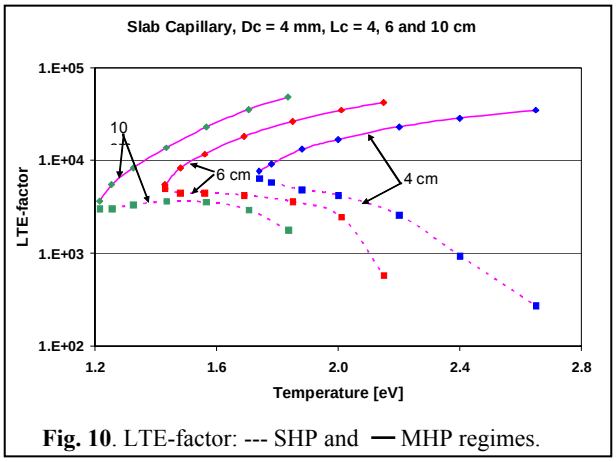

Fig. 10. LTE-factor: --- SHP and — MHP regimes.

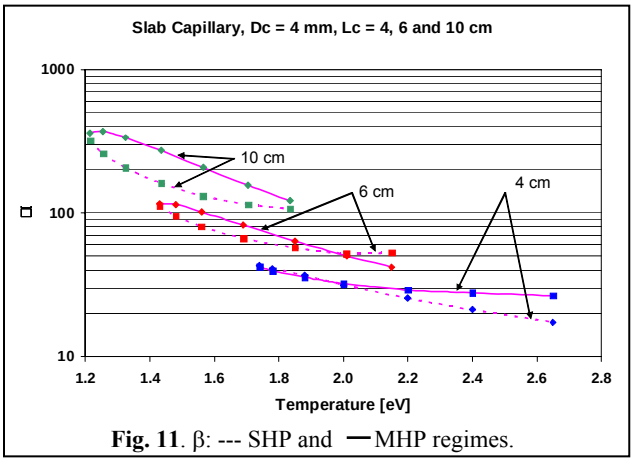

Fig. 11. β: --- SHP and — MHP regimes.

Thus, the presented model cannot adequate describe the MHP-regime in the case of relatively high temperatures, when the thermal heat conduction becomes larger than radiation heat flux at the transition layer. However, since in this regime the calculated LTE-factor and β are both much larger than 1 even when COND-factor is approximately 1, we may conclude even in the case when thermal conduction is much larger than the radiation (heat transfer of the ablative capillary discharge is controlled by thermal conductivity not by radiation) the capillary discharge can be operated at conditions when the LTE-factor and β are much larger than 1. This operating regime may be attractive for thruster applications as well as SHP-regime or MHP-regime depending on specific applications.

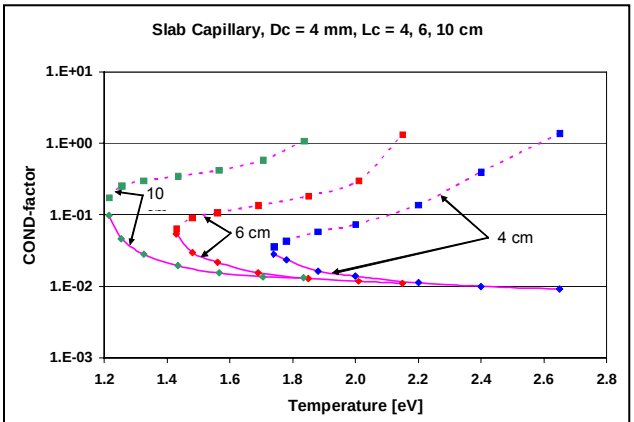

Fig. 12. Conduction factor: --- SHP and — MHP regimes.

It should be stressed, that future investigation of the stability of steady-state SHP and MHP regimes is important, and we are planning to address this issue in the future.

Acknowledgments

The author thanks Dr. J.-L. Cambier for helpful discussions during the course of present research and would like to express his gratitude to Dr. A. Pekker and M. Kapper for their kind help in preparing the text of this paper.

References

1 Tidman D. A., Y. Thio Y. C., Goldstein S. A., and Spicer D. S., "High Velocity Electrothermal Mass Launchers," GTD 86-7, GT Devices, Alexandria, VA, 1986.

2 Loeb A. and Kaplan Z., "A Theoretical model for the Physical Processes in the Confined High Pressure Discharges of Electrothermal Launchers," IEEE Trans. Magn., Vol. 25, p. 342, 1989.

3 Gilligan J. G. and Mohanti R. B., "Time-Dependent Numerical Simulation of Ablation-Controlled Arcs," IEEE Trans. Plasma Scie., Vol. 18, p. 190, 1990.

4 Powel J. D. and Zielinski A. E., "Theory and Experiment for an Ablative-Capillary Discharge and Application to Electrothermal-Chemical Guns," US Army Ballistic Res. Lab., Aberdeen Proving Ground, Tech. Rep. BRL-TR-3355, June 1992.

[5] Powel J. D. and Zielinski A. E, "Capillary Discharge in the Electrothermal Gun," IEEE Trans. Magn., Vol. 29, p. 569, 1993.
[6] Zoler D., Saphier D., and Alimi R, "A Numerical Study of the Evolution of Plasma Parameters in an Ablative Capillary Discharge for a Two-Pulse Form of Energy Input," J. Phys. D., Vol. 27, p. 142, 1994.
[7] Zoler D. and Alimi R., "A Proof of the Need for Consistent Treatment in Modeling of Capillary Ablative Discharges," J. Phys. D., Vol. 28, p. 1141, 1995.
[8] Raja L. L., Varghese P. L., and Wilson D. E, "Modeling of the Electrogun Metal Vapor Plasma Discharge," J. Thermophs. Heat Trans., Vol.11, p. 353, 1997.
[9] Shafir N., Zoler D., Wald S., and Shapiro M., "Reliable, High Reproducible Plasma Injectors for Electrothermal and Electrothermal-Chemical Launcher," IEEE Trans. Magn., Vol. 41, p. 355, 2005.
[10] Kim K., "Time-Dependent One-Dimensional Modeling of Pulsed Plasma Discharge in a Capillary Plasma Device," IEE Trans. Plasma Sci., Vol. 31, p. 729, 2003.
[11] Kim K., "Numerical Simulation of Capillary Plasma Flow Generated by High-Current Pulsed Power," International Journal of Thermal Science, Vol. 44, p. 1039, 2005.
[12] Pekker L, Cambier J.-L., "A Model of Ablative Capillary Discharge," IHTC-13, Sydney Australia, August 13-18, 2006.
[13] Cambier J.-L., Young M., Pekker L., and Pancotti A., "Capillary Discharge Based Pulsed Plasma Thruster," IEPC-2007-238, 2007.
[14] Edamitsu T. and Tahara H., "Experimental and Numerical Study of an Electrothermal Pulsed Thruster for Small Satellites," Vacuum, Vol. 80, p. 1223, 2006.
[15] Keidar M. and Boyd I. D., "Ablation Study in the Capillary Discharge of an Electrothermal Gun," J. Appl. Phys. Vol. 99, 0533301, 2006.
[16] Cros B., Courtois C., Malka G., Matthieussent G., Marques J. R. et. al., "Extending Plasma Accelerators: Guiding with Capillary Tubes," IEEE Trans Plasma. Sci., Vol 28. p.1071, 2000.
[17] Bobrova N. A., Esaulov A. A., Sakai J.-I., Sasorov P.V., Spence D. J et. al., "Simulation of Hydrogen-Filled Capillary Discharge Waveguide," Phys. Rev. E, Vol. 65, p. 016407, 2002.
[18] Spence D. J., Bulter A., and Hooker S. M., "Gas-Filled Capillary Discharge Waveguides," J. Opt. Soc. Am. B Vol. 20, p. 138, 2003.
[19] Mocek T., McKenna C. M., Cros B., Sebban S., Spence D. J. et. al., Phys. Rev. A Vol. 71, p. 013804, 2005.
[20] Prism Computational Sciences, Inc., 455 Science Drive, Suite 140, Madison, WI 53711, www.prism-sc.com.
[21] NRL Plasma Formulary, Naval Research Laboratory, Washington, DC 20375-5320.
[22] Raizer Y.P., "Gas Discharge Physics", Springer, 1997.
[23] L. Spitzer L. "Physics of Fully Ionized Gases", Chap. 5, Interscience Publisher, New York 1953.
[24] Zollweg R. J. and Liebermann R. W., "Electrical Conductivity of Nonideal Plasmas," J. Appl. Phys. Vol. 62, p. 3621, 1987.
[25] Ebeling W. and Sandig R., "Theory of the Ionization Equilibrium in Dense Plasmas," Ann Physic Vol.28, p.289, 1973.
[26] Ebeling W., Foster A., Hess H., and Romanovsky M. Yu, "Thermodynamic and Kinetic of Hot Nonideal Plasmas," Plasma Phys. Control. Fusion, Vol. 38, p. A31, 1996.
[27] Griem R.H., "High-Density Corrections in Plasma Spectroscopy," Phys. Rev. Vol. 128, p. 997, 1962.
[28] Emanuel G., "Gasdynamics: Theory and Applications," AIAA Education Series, New York, N.Y.